J. Condensed Matter Nucl. Sci. 21 (2016) 26–39

Research Article

Proton Conductors: Nanometric Cavities, H_2 Precipitates under Pressure, and Rydberg Matter Formation

François de Guerville*

i2-HMR International Institute for Hydrogen Materials Research, 56 Rue Estelle, 34 000 Montpellier, France

Abstract

Proton conductors (PC) are metal oxides often used as solid electrolyte with hydrogen above 400 K, in which anomalous presence increase of several chemical elements and excess heat would have been obtained from near-surface locations. Near the surface of other metal oxides, closely spaced hydrogen at a distance of only 2 pm at least during a fraction of the time has been detected, and has been proposed to be in the form of hypothetical ultradense Rydberg matter H(0). How can H(0) form in PC near the cathode interface? Nanometric cavities (NC) were observed in the PC near their cathode interfaces. These NC would contain H_2 precipitates with impurities, under a pressure of the order of 0.1 GPa. Since PC are crossed by a large flux of protons, a simple mechanism is proposed to increase the H_2 pressure in these NC rapidly and temporarily well above the PC tensile strength. A second mechanism is then described to turn this H_2 into a metallic-molecular state, form a Rydberg matter H(1) and then H(0) with a pressure decrease. In NC, the presence of impurities and the entry of the hydrogen atoms in the form of Rydberg atoms are proposed to decrease the pressure required to form metallic-molecular hydrogen. Finally, different experiments are proposed to test this research approach, particularly by transmission electron microscopy and Raman micro-spectroscopy.
 ISSN 2227-3123

Keywords: H_2 precipitates, Impurities, Large hydrogen flux, Nanometric cavities, Partial metallization of hydrogen, Pressure, Proton conductors, Rydberg states

1. Introduction

Some metal oxide crystals with perovskite structure are excellent Proton Conductors (PC). The PC can be used as solid electrolytes with H_2 above 400 K with porous electrodes. They are then penetrated by a very large hydrogen flux (proton conductivity up to 0.4 S/cm at 900 K) [1–3], and incorporate large concentrations of protons (several atomic percent) [4].

The PC are among the simplest and the most effective systems to study Condensed Matter Nuclear Science (CMNS). Mizuno et al. carried out CMNS experiments with polycrystalline PC based on Y-doped $SrCeO_3$ used as solid electrolytes at 650 K with deuterium passing through Pt porous electrodes, as shown in Fig. 1. Voltage and

*E-mail: francois.de.guerville@i2-hmr.com

 ISSN 2227-3123

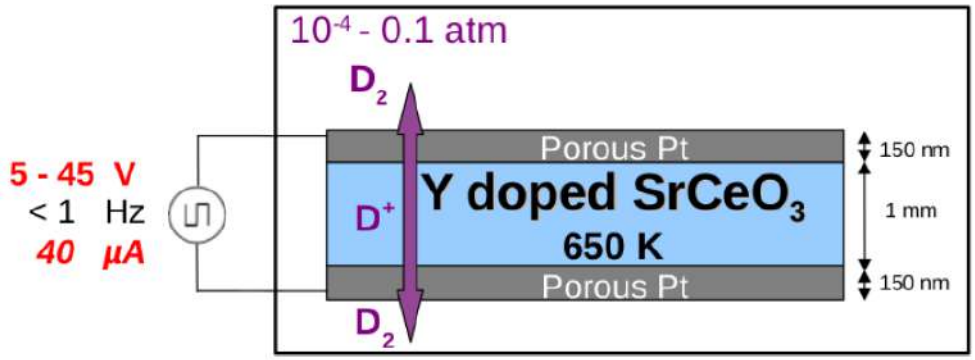

Figure 1. Mizuno's experimental system to study CMNS using a polycrystalline proton conductor based on Y-doped $SrCeO_3$ as solid electrolyte with D_2. From [8].

intensity were as low as 18 V and 40 μA. The unit cell of Y-doped $SrCeO_3$ keeps a centrosymmetric structure and thus there is no additional electric polarization of the material which could give additional kinetic energy to the hydrogen ions. Mizuno et al. have reported the observation of chemical elements in the PC near their electrode interfaces which were not present before electrolysis [5,6], and anomalous heat production during electrolysis [7–9], as shown in Fig. 2. Similar results were reported by other researchers with other PC [10–12].

Holmlid and coworkers' experiments have shown that, near the surface of highly porous metal oxide crystals based on K-doped Fe_2O_3 exposed to hydrogen, a part of the hydrogen atoms are separated from each other by only 2 pm at least during a fraction of time, as shown in Fig. 3a [13–18]. Other experiments are consistent with the presence of a significant population of compact pairs of hydrogen atoms in other hydrogenated materials [19]. This closely spaced hydrogen might be a new form of hydrogen, called H(0), shown in Fig. 3b. H(0) is a hypothetical ultradense form of Rydberg matter with a phenomenal density of 10^5 g/cm^3. It might be a promising nuclear fuel, superfluid

Element	Before experiment	No excess heat	Excess heat evolved
Li	5 ± 0.7	5 ± 0.7	5 ± 1
Na	10 ± 1	10 ± 1	12 ± 1
Mg	5 ± 0.8	5 ± 1.2	10 ± 3
K	10 ± 0.9	10 ± 1.5	15 ± 1.8
Ca	20 ± 2	20 ± 0.8	40 ± 5
Ba	40 ± 5	40 ± 8	40 ± 10
Al	3 ± 0.2	5 ± 1	15 ± 5
Si	1.5 ± 0.1	3 ± 1	5 ± 1
Fe	0.5 ± 0.1	3 ± 1	5 ± 1
Ni	2 ± 0.1	3 ± 1	5 ± 1
Cu	0.3 ± 0.1	1 ± 1	1 ± 1
Cr	1 ± 0.1	2 ± 1	2 ± 1
Cd	0.5 ± 0.1	1 ± 0.5	1 ± 0.5
Pd	6.5 ± 1	6 ± 1	8 ± 2
Bi	0	0.1	5 ± 1
Zn	0.5 ± 0.1	1 ± 0.1	2 ± 0.2
Nd	2.5 ± 0.1	2.5 ± 0.1	4 ± 1
Sm	2.0 ± 0.1	2.0 ± 0.1	10 ± 1
Gd	0	0	5 ± 1
Dy	0	0	5 ± 1

(a)

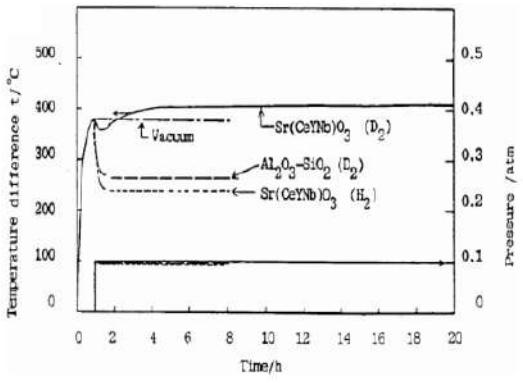

(b)

Figure 2. (a) Elemental analysis for impurities in the proton conductor Y-doped $SrCeO_3$, showing the presence increase of several chemical elements after electrolysis. (b) Anomalous heat production during electrolysis. From [6,8].

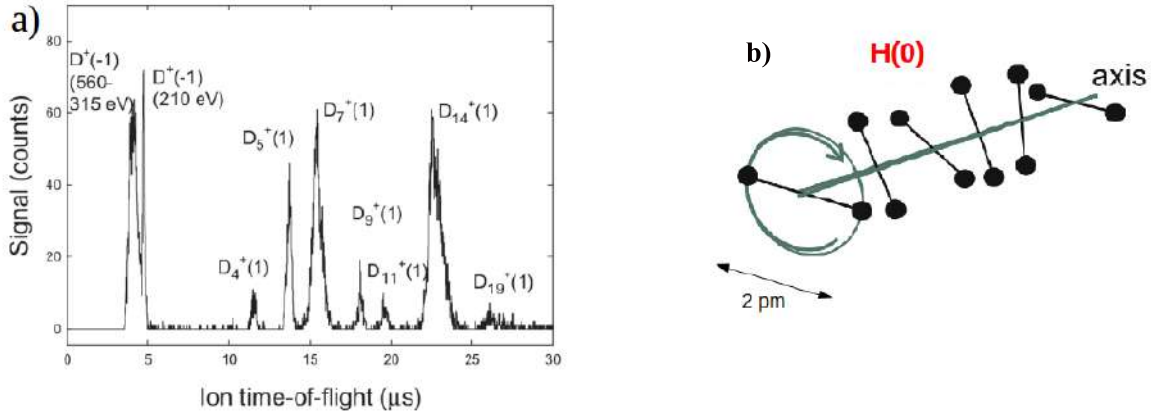

Figure 3. (a) Laser induced Coulomb explosions with time-of-flight mass spectroscopy near the surface of a metal oxide based on K-doped Fe_2O_3. The two first peaks correspond to closely spaced deuterons (2 pm). From [13]. (b) Hypothetical ultradense hydrogen Rydberg matter H(0). From [18].

and superconductive at room temperature. The presence of H(0) in a PC near its cathode interface could explain the observation of new chemical elements and excess heat.

H(0) would form almost spontaneously from classical hydrogen Rydberg matter H(1). H(1) can be viewed as a generalized metal [20–24]. Moreover, H(0) could be formed directly from H_2 at ultrahigh pressures. Thus, the route explored in this article points toward metallization of hydrogen and high pressures. The main question of this article is: How to form hydrogen Rydberg matter in a PC used as solid electrolyte with H_2 at 650 K near its cathode interface?

2. State of the Art in Condensed Matter Physics

2.1. Nanometric cavities and H_2 precipitates under pressure

There has not been much research into nanoscale structure of PC with large densities of incorporated protons. However, crystalline silicon and metal oxides with perovskite structure implanted by large quantities of protons have been intensely studied, and this knowledge can be adapted to PC.

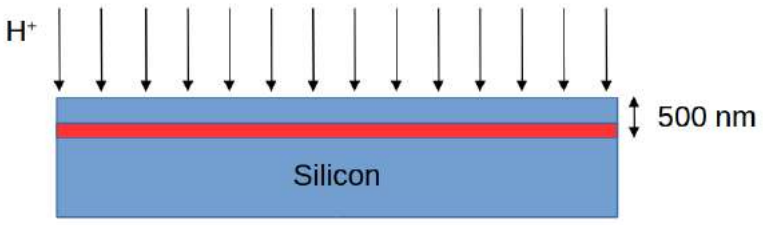

Figure 4. Ionic implantation of H^+ in silicon crystals.

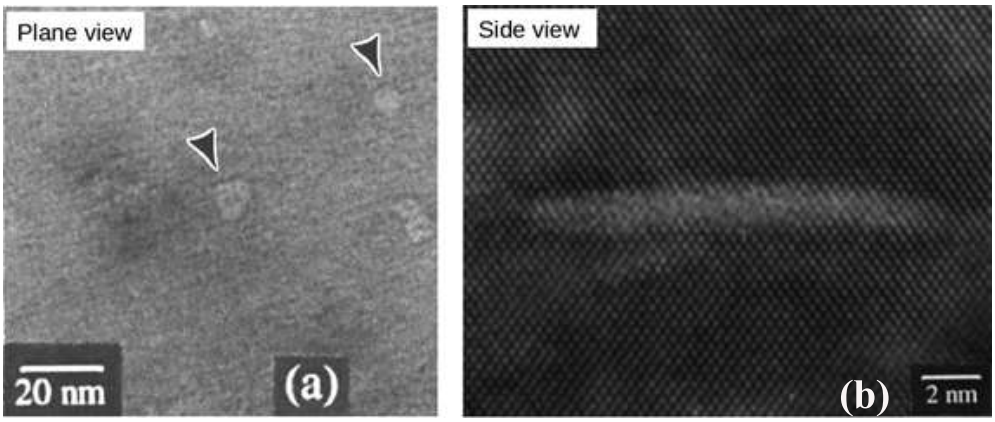

Figure 5. Nanometric cavities in H^+ implanted silicon, after an annealing at 720 K, observed by TEM. (a) Plane view and (b) cross-section side view. From [26].

2.1.1. *In silicon implanted with H^+*

Silicon does not conduct protons. With the ionic implantation technique, crystal surfaces are temporarily penetrated by a large flux of hydrogen ions. This technique is used to obtain large hydrogen local concentrations in these materials, typically at a depth of several hundred nanometers under the surface, as shown in Fig. 4. During material implantation, many point defects are created among which vacancy-hydrogen complexes V_nH_m [25].

During annealing, when hydrogen concentration locally overtakes the solubility limit, these mobile complexes V_nH_m agglomerate to form disk-shaped cavities of about ten nanometers in diameter [26–28]. This co-precipitation of vacancies and hydrogen, followed by the competitive growth ("Ostwald ripening") of the Nanometric Cavities (NC) and their coalescence, allow the crystalline matrix-defects system to minimize its elastic energy. Such NC are observable by Transmission Electron Microscopy (TEM) after an annealing at 720 K [26]. Figure 5a shows some NC in their disc plane (plane view). Figure 5b, obtained from a TEM cross-section of the sample, shows a NC perpendicularly

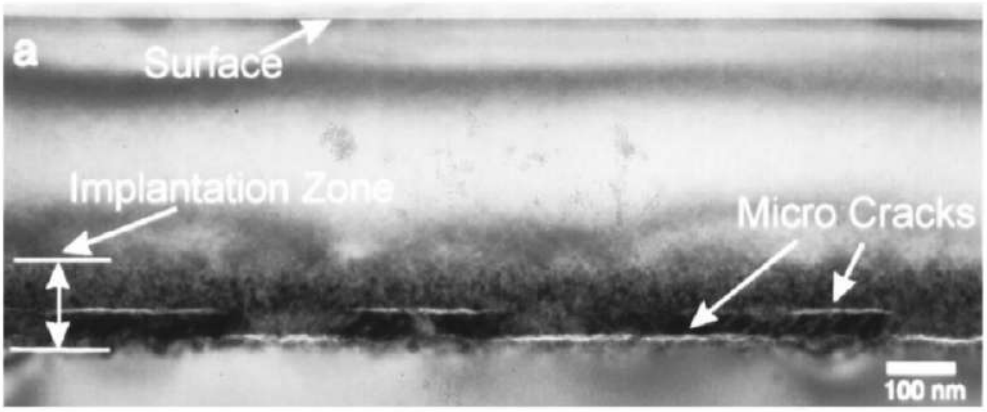

Figure 6. Nanometric cavities in H^+ implanted silicon, after an annealing at 870 K for 30 min, observed by cross-sectional TEM. From [29].

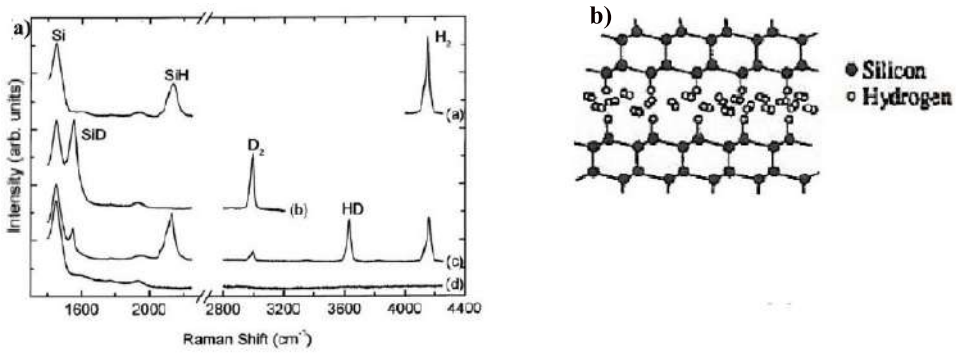

Figure 7. (a) Raman spectroscopy on Si surface implanted with hydrogen ions at 470 K showing the presence of H_2 molecules in nanometric cavities. From [31]. (b) Diagram of H_2 molecules trapped in Si nanometric cavities. From [29].

to its disc plane (side view). Figure 6 shows microcracks formed from a large density of NC in the implantation zone after an annealing at 870 K [29].

These NC contain precipitates of molecular hydrogen H_2 [29–32]. They are traps for hydrogen and for impurities [33], and they contain most of the implanted hydrogen [32]. The presence of H_2 in these NC was established by Raman spectroscopy. In Fig. 7a, the top Raman spectrum is composed of three peaks. The first two correspond to Si–Si and Si–H vibrations. The third one corresponds to the H–H vibration of H_2 (vibron) and has a characteristic position when the H_2 is fluid, as it is the case here [30,31]. Figure 7b shows hydrogen molecules H_2 in a NC [29].

The H_2 filling a NC is typically pressured to a dozen of GPa at 300 K [34–37]. This value is above the tensile strength of silicon, around 7 GPa. It is expected that this internal pressure of H_2 is much larger during annealing above 650 K [34]. This pressure decreases when the diameter of the NC increases. Reciprocally, this H_2 under pressure generates stress on the crystalline matrix. The resulting strain field contrast surrounding a NC can be observed by TEM, as shown in Fig. 8a [28]. A diagram showing the pressure of H_2 in NC on the Si crystalline matrix is presented in Fig. 8b [29].

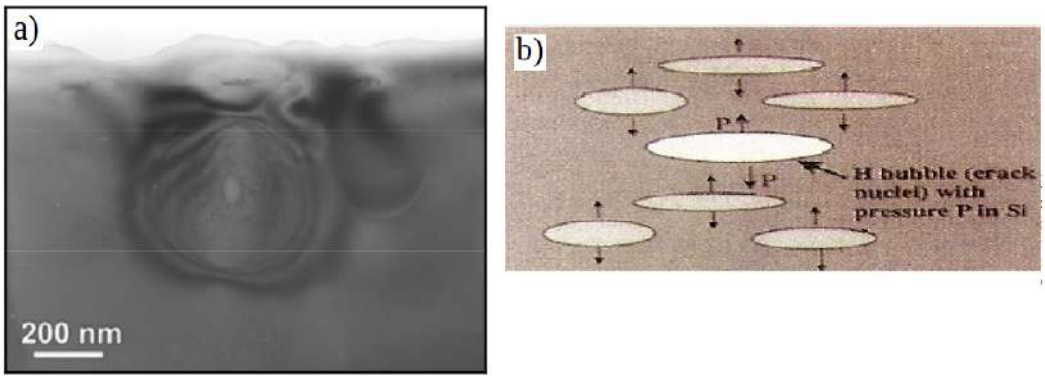

Figure 8. (a) Cross-section TEM image showing a nanometric cavity pressurized by its internal H_2, and the long-range surrounding strain field, deep under the free surface of a hydrogenated Si wafer below 470 K. From [28]. (b) Diagram showing the pressure of H_2 in nanometric cavities on the Si crystalline matrix. From [29].

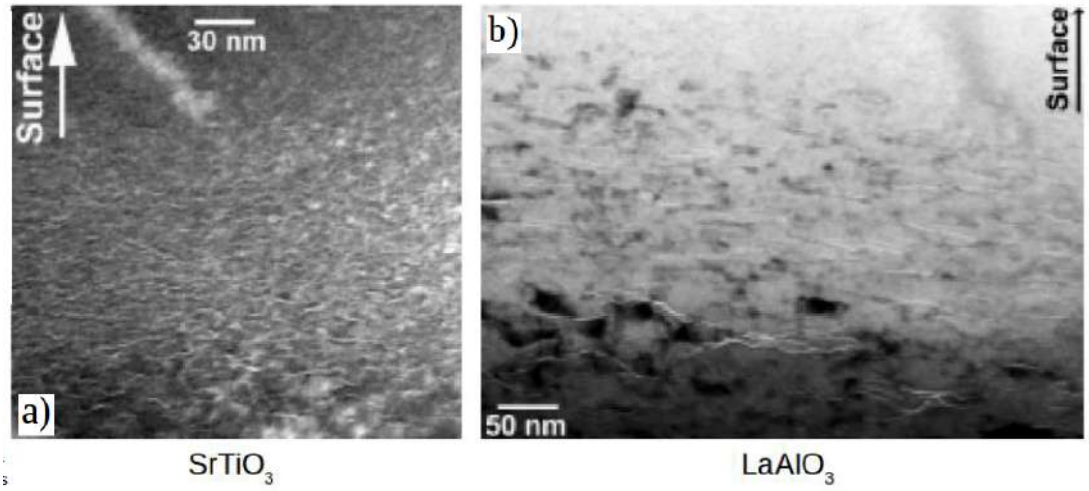

Figure 9. TEM images of high local densities of hydrogen related nanometric cavities (*side view*) in metal oxides with perovskite structure near their surfaces. These samples were implanted with hydrogen at 300 K for $SrTiO_3$ (a) and 570 K for $LaAlO_3$ (b). From [38].

2.1.2. *In metal oxides with perovskite structure implanted with H^+*

The same phenomena are observed in metal oxides with perovskite structure, such as $SrTiO_3$, $BaTiO_3$, $LaAlO_3$ and $LiTaO_3$ [38–40]. The two TEM images in Fig. 9 show large densities of NC under the surfaces of $SrTiO_3$ and $LaAlO_3$ [38].

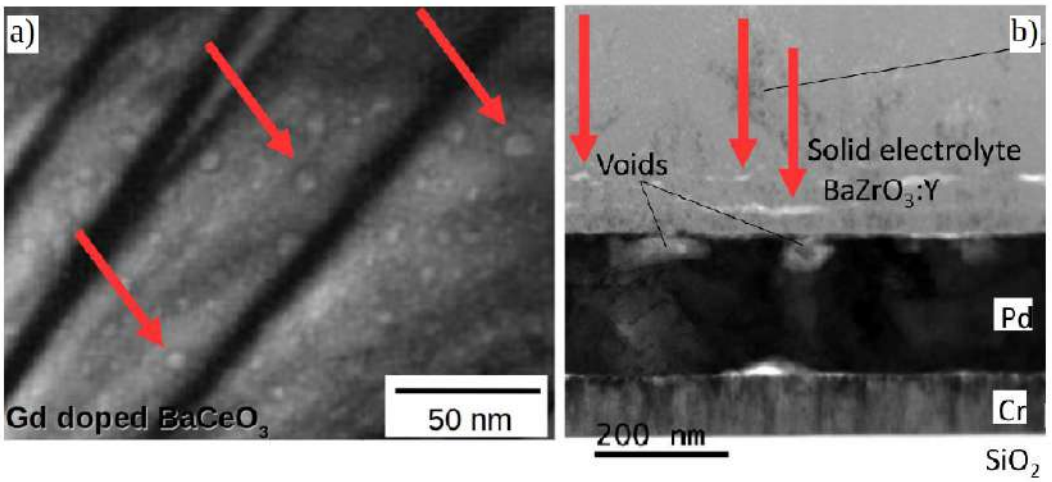

Figure 10. TEM images of nanometric cavities in polycrystalline proton conductors. Red arrows highlight some nanometric cavities. (a) Plane view in Gd-doped $BaCeO_3$ used below 770 K. From [41]. (b) Cross-section side view in Y-doped $BaZrO_3$ used at 590 K. From [42].

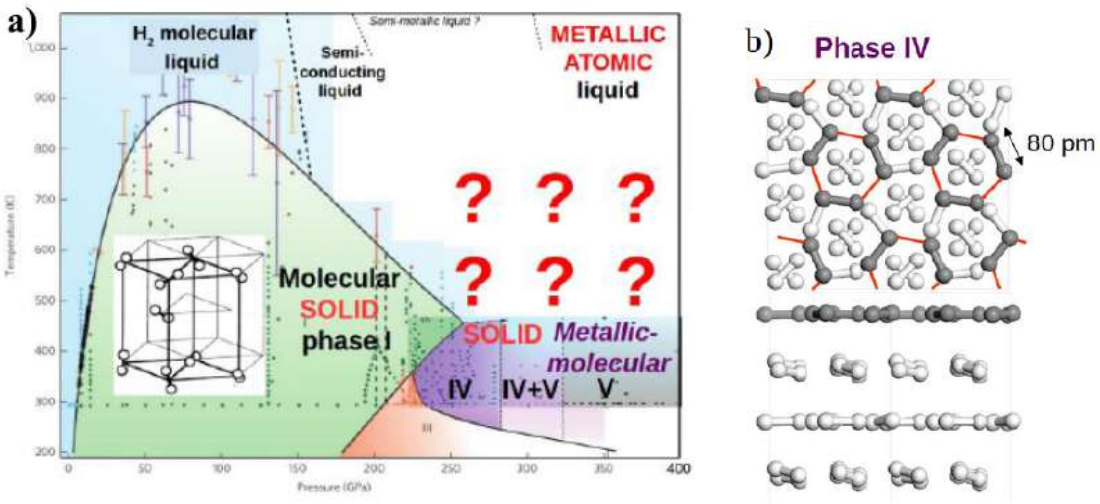

Figure 11. (a) Phase diagram $P - T$ of pure hydrogen, established by Raman spectroscopy. From [44, 46–51]. (b) Metallic-molecular phase IV of hydrogen. From [51].

In hydrogen-implanted $BaTiO_3$, the internal pressure of H_2 in microcracks was evaluated between 0.004 and 0.5 GPa [39]. This pressure should be considerably higher in NC. The tensile strength of polycrystalline $BaTiO_3$ is 0.06 GPa.

2.1.3. *In proton conductors used as solid electrolytes with hydrogen*

High densities of NC related to hydrogen incorporation have been observed by TEM in three polycrystalline PC used as solid electrolytes with hydrogen [41–43]. Figure 10 shows TEM images of Gd-doped $BaCeO_3$ used below 770 K (Fig. 10a) and Y-doped $BaZrO_3$ used at 590 K (Fig. 10b). For Y-doped $BaZrO_3$, these NC were found within a depth

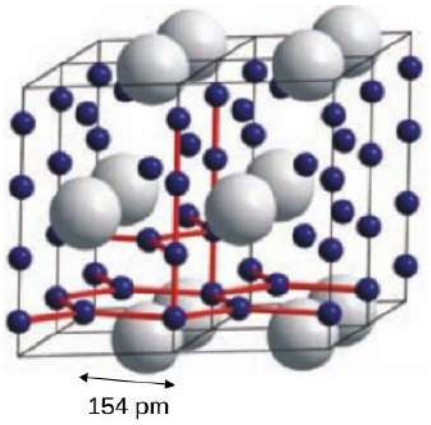

Figure 12. Fully metallic phase of SiH_4 at only 113 GPa at 300 K. From [53].

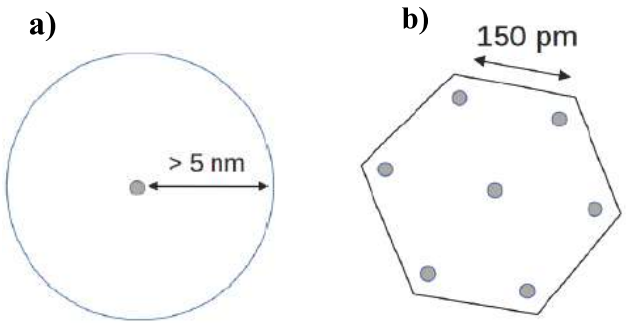

Figure 13. (a) Hydrogen Rydberg atom. (b) Hydrogen Rydberg matter H(1).

of 100 nm from its cathode interface, whereas for $Ba_3Ca_{1.18}Nb_{1.82}O_{9-\delta}$ used at 1020 K, these NC were found in its grain boundaries.

The phenomena observed in PC near their cathode interface when they are used as solid electrolyte with hydrogen at around 650 K can be similar to those observed in silicon and in metal oxides with perovskite structure implanted with H^+.

2.2. Partial metallization of hydrogen

2.2.1. *Hydrogen with impurities under high pressures*

Pure hydrogen can be compressed to high pressures in disk-shaped diamond anvil cells, whose dimensions are typically 100 μm in diameter and 5 μm in thickness [44–49]. The pressure–temperature phase diagram of hydrogen, obtained by Raman spectroscopy, is presented in Fig. 11a [44,46–51]. Hydrogen is a molecular solid in phase I above 5 GPa at 300 K, and above 23 GPa at 650 K. Above 250 GPa at 650 K, the phase of hydrogen has not been studied yet.

Above 250 GPa and at 300 K, hydrogen is a metallic-molecular solid in phase IV and/or V. As shown in Fig. 11b, the structures of these phases are constituted of alternating layers of :

(1) H_2 molecules forming sheets of graphene type by intermolecular coupling, and whose state is intermediate between metallic state and molecular state,
(2) normal hydrogen molecules H_2.

In metallic-molecular H_2, the intramolecular length of H_2, initially equal to 74 pm, increases with pressure [51].

Although whether it is possible to produce metallic hydrogen in the laboratory is still debated, above 450 GPa and at room temperature (not shown), hydrogen is supposed to be fully metallic and superconducting.

The presence of some impurities (Li, Si, S, ...) significantly decreases the pressure required to approach a metallic state when hydrogen is compressed in a diamond anvil cell [52–55]. Figure 12 shows the structure of metallic SiH_4 under 113 GPa at 300 K, but SiH_4 is fully metallic above only 50 GPa [53]. In this configuration, hydrogen atoms are separated from each other by 154 pm.

2.2.2. *Rydberg states*

Different Rydberg states are shown in Fig. 13. A hydrogen Rydberg atom (Fig. 13a) is a hydrogen atom with its electron orbiting very far from the proton (> 5 nm), quasi-circularly [56]. It results from recombination of a proton

and an electron, and it easily forms on metal oxide surfaces.

Hydrogen Rydberg matter H(1) is a hexagonal plane cluster of circular Rydberg atoms (Fig. 13b), whose electrons are strongly excited and delocalized [20–24]. In this phase, hydrogen is a generalized metal which has properties similar to covalent bonding. Protons are separated from each other by 150 pm at the fundamental energy level.

3. Research Approach

3.1. Rapid and temporary increase of H_2 pressure in nanometric cavities of proton conductors

This research approach starts with the facts that PC, submitted to electrolysis with H_2 at 650 K, can contain a high local density of NC near their cathode interfaces and are crossed by a large flux of hydrogen.

Hypothesis 1: The NC contain $\mathbf{H_2}$ and hydrogen combined with impurities under a pressure on the order of 0.1 GPa.

Hypothesis 2: The NC are penetrated by a large flux of hydrogen.

Hypothesis 3: The entering hydrogen is trapped in the NC in the form of $\mathbf{H_2}$, and the outgoing hydrogen flux is negligible compared to the entering flux.

Hypothesis 4: The internal pressure of the hydrogen in the NC increases rapidly and temporary well above the PC tensile strength. The questions arising from this hypothesis are discussed in Section 4.1.

3.2 Ultradense Rydberg matter formation in nanometric cavities of proton conductors with decrease of H_2 pressure

From now on, H(0) is supposed to exist and to possibly form in PC. The proposed H(0) formation mechanism is illustrated in Fig. 14.

Hypothesis 5: In NC with a diameter greater than 40 nm, hydrogen penetrates in the form of circular Rydberg atoms ($n \geq 20, l = m = n - 1$).

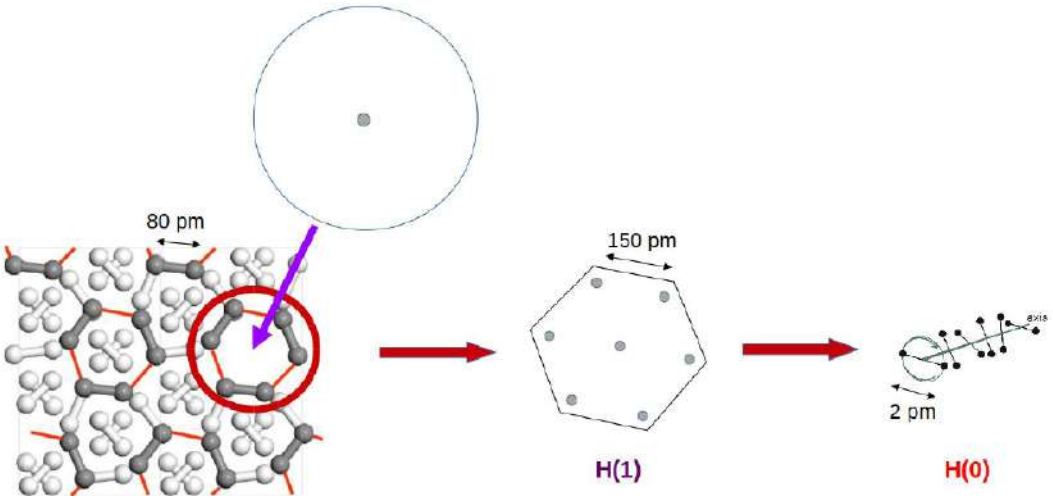

Figure 14. Proposed mechanism for H(1) formation in nanometric cavities consisting of circular hydrogen Rydberg atoms bombarding metallic-molecular hydrogen sheets, followed by the formation of the hypothetical H(0) and decrease of pressure.

Hypothesis 6: The H_2 with impurities in the NC turns temporarily into a metallic-molecular phase. The required temporary internal pressure could be only on the order of tens GPa.

Hypothesis 7: Circular Rydberg atoms penetrating into the NC transfer their excitation energy to the metallic-molecular sheets of H_2 in the immediate proximity of the NC wall, and together, they turn into Rydberg matter H(1).

Hypothesis 8: H(1) spontaneously turns into H(0) under the conditions prevailing in the NC. This transition is accompanied by a pressure decrease in the NC.

4. Discussion

4.1. Rapid and temporary increase of H_2 pressure in nanometric cavities well above the tensile strength of the proton conductor

It should take less than 1 min to increase the pressure of pure hydrogen from 0.1 to 20 GPa at 650 K, in a disk-shaped NC with a thickness of 1.5 nm penetrated by a flux of five hydrogen atoms per nm^2 per second at normal incidence, regardless of its diameter [57]. Nowadays, better PC (for instance, Y-doped $BaZrO_3$ single crystals) can achieve much larger fluxes than the one considered here, estimated from [8]. Otherwise, since NC trap impurities, they might acquire a global electrical charge, and the incoming proton flux in NC might be different from what was envisaged.

In NC, what mechanisms limit this pressure increase? From what is known for H^+ implanted silicon during annealing, H_2 pressure increase in NC should accelerate the NC growth by Ostwald ripening. Yet, the mechanical properties of the crystalline matrix change locally within the vicinity of a single pressurized NC [39]. Pressurized NC could implement compressive stress on the nearby PC matrix, thus having an inhibiting effect on the growth on each other [29].

Morevover, H_2 pressure increase in NC should accelerate the coalescence of a tiny part of the NC into microcracks, in which the internal pressure is lower. At a given annealing temperature, depending on the local concentration of hydrogen, the characteristic time needed to form microcracks can be on the order of 1 h. Consequently, the proposed rapid internal pressure increase may be little limited by the slower NC coalescence into microcracks. Finally, an open question is: Why have only Samgin et al. [11] reported the observation of cracks in their PC samples after CMNS experiments?

4.2. Rydberg matter formation

Other open questions follow. Is it possible to decrease the pressure required for partial metallization of hydrogen in NC down to several tens of GPa, thanks to the presence of impurities and the entry of hydrogen atoms in NC in the form of Rydberg atoms?

What is the NC optimum size to form H(1)? If the NC are too small, circular Rydberg atoms cannot enter them. If they are too large, the H_2 internal pressure may be too low to turn H_2 into metallic-molecular phase. I propose 40 nm in diameter and 1.5 nm in thickness is the optimum size. The best NC orientation should be parallel to the interfaces. Furthermore, could the formation of H_2 Rydberg molecules [58] play a role in H(1) formation?

5. Experimental Tests to Validate this Approach

5.1. Transmission electron microscopy

The TEM is the best tool to observe NC in a crystalline matrix, and study their locations, their sizes, their shapes, their orientations and their density. Strain field contrast is also observable around NC containing hydrogen under pressure.

Together with simulations, it is possible to deduce the H_2 pressure within the NC [34]. The TEM with electron energy-loss spectroscopy enables accurate mapping of hydrogen in the samples, and provides information on its bounding [59,60].

5.2. Raman micro-spectroscopy

Raman micro-spectroscopy reveals hydrogen vibrations and is the most adapted tool to detect the presence of H_2 with impurities trapped in the NC near the cathode interface. Moreover, this technique enables us to identify and study the hydrogen phase: molecular fluid, molecular solid, metallic-molecular solid, or Rydberg matter H(1). For H(1), it is possible to study electronic excitation and vibrational shifts of its partially covalent bonding [20]. However, the presence of impurities in the NC should complicate the deciphering of the Raman spectra. It may then be difficult to identify the hydrogen phase and evaluate its internal pressure.

Otherwise, stresses undergone by the crystalline matrix, generated by H_2 in the NC, are also roughly assessable by Raman spectroscopy.

Sample structural characterizations under the surface up to a depth of about 1 μm can be carried out, after removing the cathode by chemical etching in an acid bath. By using a laser excitation wavelength below the optical absorption threshold, the probed depth can be decreased to about several hundreds of nm or less [61], which is the ideal depth to probe the NC. Furthermore, the use of confocal microscopy also limits the probed depth to $\sim$500 nm.

5.3. X-ray diffraction

X-ray diffraction enables us to measure strain perpendicular to the surface plane in a layer of a crystalline matrix, generated by a large density of in-plane NC containing H_2 under pressure. These measurements can be carried out in-situ [42]. Probed depth is around 2 μm.

5.4. Neutron scattering

Neutron diffraction can detect long range ordered structure of deuterium. It does not work so well on protium, due to its lower mass. If there is enough ordered deuterium in NC, a deuterium lattice may be detectable inside. Moreover, information could be obtained about the molecular dynamics and the collective dynamics of hydrogen (phonons) in NC. Yet, the probed depth is very large and the bulk of the sample is probed.

5.5. Nuclear magnetic resonance spectroscopy

An NMR spectrum with anomalously large shift in a proton NMR experiment would provide unambiguous independent confirmation of the presence of closely spaced hydrogen.

5.6. Laser-induced Coulomb explosions with time-of-flight mass spectroscopy

This technique allows to detect closely spaced hydrogen near a material surface, and evaluate the initial distance between them.

6. Conclusion

In proton conductors, used as solid electrolytes with hydrogen around 650 K, large densities of nanometric cavities can form near their cathode interfaces. Assuming these nanometric cavities contain H_2 precipitates with impurities under

a pressure on the order of 0.1 GPa, a simple mechanism is proposed to increase rapidly and temporarily the H_2 internal pressure well above the tensile strength of proton conductors. Then, assuming hydrogen can exist as ultradense H(0), a second mechanism is proposed to make the H_2 with impurities in the nanometric cavities turn into a metallic-molecular phase, form Rydberg matter H(1) and then form H(0) with a pressure decrease. In nanometric cavities, the presence of impurities and the entry of the hydrogen atoms in the form of Rydberg atoms are proposed to decrease the pressure required to form metallic-molecular hydrogen. Different experiments are proposed to study the hydrogen trapped in these nanometric cavities, particularly by transmission electron microscopy and Raman micro-spectroscopy.

References

[1] A. Braun, A. Ovalle, V. Pomjakushin, A. Cervellino and S. Erat, Yttrium and hydrogen superstructure and correlation of lattice expansion and proton conductivity in the $BaZr_{0.9}Y_{0.1}O_{2.95}$ proton conductor, *Appl. Phys. Lett.* **95** (2009) 224103.

[2] D. Pergolesi, E. Fabbri, A. D′Epifanio, E. Di Bartolomeo, A. Tebano, S. Sanna, S. Licoccia, G. Balestrino and E. Traversa, High proton conduction in grain-boundary-free yttrium-doped barium zirconate films grown by pulsed laser deposition, *Nat. Mater.* **9** (2010) 846.

[3] Y.B. Kim, T.M. Gür, H.J. Jung, S. Kang, R. Sinclair and F.B. Prinz, Effect of crystallinity on proton conductivity in yttrium-doped barium zirconate thin films, *Solid State Ionics* **198** (2011) 39.

[4] M. Glerup, F.W. Poulsen and R.W. Berg, Vibrational spectroscopy on protons and deuterons in proton conducting perovskites, *Solid State Ionics* **148** (2002) 83.

[5] T. Mizuno, K. Inoda, T. Akimoto, K. Azumi, M. Kitaichi, K. Kurokawa, T. Ohmori and M. Enyo, Anomalous gamma peak evolution from SrCe solid state electrolyte charged in D_2 gas, *Int. J. Hydrogen Energy* **22** (1997) 23.

[6] T. Mizuno, T. Akimoto, K. Azumi, M. Kitaichi, K. Kurokawa and M. Enyo, Excess heat evolution and analysis of elements for solid state electrolyte in deuterium atmosphere during applied electric field, *J. New Energy* **1**(1) (1996) 79.

[7] T. Mizuno, T. Akimoto, K. Azumi, M. Kitaichi, K. Kurokawa and M. Enyo, Anomalous heat evolution from a solid-state electrolyte under alternating current in high-temperature D_2 gas, *Fusion Sci. Technol.* **29** (1996) 385.

[8] T. Mizuno, M. Enyo, T. Akimoto and K. Azumi, Anomalous heat evolution from $SrCeO_3$-type proton conductors during absorption/desorption of deuterium in alternate electric field, *Proc. ICCF4* **2** (1993) 14-1.

[9] R.A. Oriani, An investigation of anomalous thermal power generation from a proton-conducting oxide, *Fusion Sci. Technol.* **30** (1996) 281.

[10] K.A. Kaliev, A.N. Baraboshkin, A.L. Samgin, E.G. Golikov, A.L. Shalyapin, V.S. Andreev and P.I. Golubnichiy, Reproducible nuclear reactions during interaction of deuterium with oxide tungsten bronze, *Phys. Lett. A* **172** (1993) 199.

[11] A.L. Samgin, O. Finodeyev, S.A. Tsvetkov, V.S. Andreev, V.A. Khokhlov, E.S. Filatov, I.V. Murygin, V.P. Gorelov and S.V. Vakarin, Cold fusion and anomalous effects in deuteron conductors during non-stationary high-temperature electrolysis, *Proc. ICCF5* **2** (1995) 201.

[12] J.-P. Biberian, G. Lonchampt, L. Bonnetain and J. Delepine, Electrolysis of $LaAlO_3$ single crystals and ceramics in a deuteriated atmosphere, *Proc. ICCF7* (1998) 27.

[13] S. Badiei, P.U. Andersson and L. Holmlid, Production of ultradense deuterium: a compact future fusion fuel, *Appl. Phys. Lett.* **96** (2010) 124103.

[14] F. Olofson and L. Holmlid, Detection of MeV particles from ultra-dense protium p(–1): laser-initiated self-compression from p(1), *Nucl. Instr. Meth. Phys. Res. B* **278** (2012) 34.

[15] L. Holmlid, Excitation levels in ultra-dense hydrogen p(-1) and d(-1) clusters: structure of spin-based Rydberg matter, *Int. J. Mass Spectrom.* **352** (2013) 1.

[16] L. Holmlid and S. Fuelling, Meissner effect in ultra-dense protium p($l = 0$, $s = 2$) at room temperature: superconductivity in large clusters of spin-based matter, *J. Cluster Sci.* **26** (2015) 1153.

[17] L. Holmlid and S. Olafsson, Spontaneous ejection of high-energy particles from ultra-dense deuterium D(0), *Int J. Hydrogen Energy* **40** (2015) 10559.

[18] L. Holmlid and B. Kotzias, Phase transition temperatures of 405–725 K in superfluid ultra-dense hydrogen clusters on metal surface, *AIP Advances* **6** (2016) 045111.

[19] J. Kasagi, T. Ohtsuki, K. Ishii and M. Hiraga, Energetic protons and α particles emitted in 150-keV deuteron bombardment on deuterated Ti, *J. Phys. Soc. Jpn.* **64**(3) (1995) 777.

[20] L. Holmlid, Observation of the unidentified infrared bands in the laboratory: anti-stockes stimulated Raman spectroscopy of a Rydberg matter surface boundary layer, *Astrophys. J.* **548** (2001) L249.

[21] L. Holmlid, Conditions for forming Rydberg matter: condensation of Rydberg states in the gas phase versus at surfaces, *J. Phys.: Condens. Matter* **14** (2002) 13469.

[22] J. Wang and L. Holmlid, Rydberg matter clusters of hydrogen $(H_2)^*_N$ with well defined kinetic energy release observed by neutral time-of-flight, *Chem. Phys.* **277** (2002) 201.

[23] S. Badiei and L. Holmlid, Lowest state $n = 1$ of H atom Rydberg matter: many eV energy release in Coulomb explosions, *Phys. Lett. A* **327** (2004) 186.

[24] S. Badiei and L. Holmlid, Experimental observation of an atomic hydrogen material with H–H bond distance of 150 pm suggesting metallic hydrogen, *J. Phys.: Condens. Matter* **16** (2004) 7017.

[25] N. Cherkashin, F.-X. Darras, P. Pochet, S. Reboh, N. Ratel-Ramond and A. Claverie, Modelling of point defect complex formation and its application to H^+ ion implanted silicon, *Acta Mater.* **99** (2015) 187.

[26] J. Grisolia, G. Ben Assayag, A. Claverie, B. Aspar, C. Lagahe and L. Laanab, A transmission electron microscopy quantitative study of the growth kinetics of H platelets in Si, *Appl. Phys. Lett.* **76** (2000) 852.

[27] X. Hebras, P. Nguyen, K.K. Bourdelle, F. Letertre, N. Cherkashin and A. Claverie, Comparison of platelet formation in hydrogen and helium-implanted silicon, *Nucl. Instr. Meth. Phys. Res. B* **262** (2007) 24.

[28] C. Ghika, L.C. Nistor, B. Mironov and S. Vizireanu, Hydrogen-plasma induced platelets and voids in silicon wafers, *Rom. Rep. Phys.* **62 (**2010) 329.

[29] T. Höchbauer, A. Misra, M. Nastasi and J.W. Mayer, Physical mechanism behind the ion-cut in hydrogen implanted silicon, *J. Appl. Phys.* **92** (2002) 2335.

[30] K. Murakami, N. Fukata, S. Sasaki, K. Ishioka, M. Kitajima, S. Fujimura, J. Kikuchi and H. Haneda, Hydrogen molecules in crystalline silicon treated with atomic hydrogen, *Phys. Rev. Lett.* **77**(15) (1996) 3161.

[31] A.W.R. Leitch, J. Weber and V. Alex, Formation of hydrogen molecules in crystalline silicon, *Materials Sci. Eng. B* **58** (1999) 6.

[32] N. Cherkashin, N. Daghbouj, F.-X. Darras, M. Fnaiech and A. Claverie, Cracks and blisters formed close to a silicon wafer surface by He–H co-implantation at low energy, *J. Appl. Phys.* **118** (2015) 245301.

[33] B. Mohadjeri, J.S. Williams and J. Wong-Leung, Gettering of nickel to cavities in silicon introduced by hydrogen implantation, *Appl. Phys. Lett.* **66** (1995) 1889.

[34] J. Grisolia, G. Ben Assayag, B. de Mauduit and A. Claverie, TEM measurement of hydrogen pressure within a platelet, *Materials Res. Soc. Proc.* **681** (2001) I3.2.

[35] X.-Q. Feng and Y. Huang, Mechanics of Smart-Cut(R) technology, *Int. J. Solids Structures* **41** (2004) 4299.

[36] B. Aspar, C. Lagahe, H. Moriceau, A. Soubie, E. Jalaguier, B. Biasse, A. Papon, A. Chabli, A. Claverie, J. Grisolia, G. Ben Assayag, T. Barge, F. Letertre and B. Ghyselen, Smart-Cut(R) process: an original way to obtain thin films by ion implantation, *Int. Conf. Ion Implantation Technol. Proc.* (2000) 255.

[37] S. Muto, S. Takeda and M. Hirata, Hydrogen-induced platelets in silicon studied by transmission electron microscopy, *Philosophical Magazine A* **72** (1995) 1057.

[38] I. Radu, I. Szafraniak, R. Scholz, M. Alexe and U. Gösele, Ferroelectric oxide single-crystalline layers by wafer bonding and hydrogen/helium implantation, *Mat. Res. Soc. Symp. Proc.* **748** (2003) U11-8-1.

[39] Y.-B. Park, P. Nardi, X. Li and H.A. Atwater, Nanomechanical characterization of cavity growth and rupture in hydrogen-implanted single-crystal $BaTiO_3$, *J. Appl. Phys.* **97** (2005) 074311.

[40] T. Luo, T. Oda, Y. Oya and S. Tanaka, IR observation on O-D vibration in $LiNbO_3$ and $LiTaO_3$ single crystal irradiated by 3 keV D_2^+, *J. Nucl. Mater.* **382** (2008) 46.

[41] S.M. Haile, D.L. West and J. Campbell, The role of microstructure and processing on the proton conducting properties of gadolinium-doped barium cerate, *J. Materials Res.* **13** (1998) 1576.
[42] Y. Fukada, T. Hioki, T. Motohiro and S. Ohshima, In situ X-ray diffraction study of crystal structure of Pd during hydrogen isotope loading by solid-state electrolysis at moderate temperature, *J. Alloys Compounds* **647** (2015) 221.
[43] T. Schober, H.G. Bohn, T. Mono and W. Schilling, The high temperature proton conductor $Ba_3Ca_{1.18}Nb_{1.82}O_{9-\delta}$ Part II: electrochemical cell measurements and TEM, *Solid State Ionics* **118** (1999) 173.
[44] H.-K. Mao and R.J. Hemley, Ultra-high pressure transitions in solid hydrogen, *Rev. Modern Phys.* **66** (1994) 671.
[45] M.I. Eremets and I.A. Troyan, Conductive dense hydrogen, *Nat. Mater.* **10** (2011) 927.
[46] C.-S. Zha, R.E. Cohen, H.-K. Mao and R.J. Hemley, Raman measurements of phase transitions in dense solid hydrogen and deuterium to 325 GPa, *Proc. Natl. Acad. Sci. U.S.A.* **111** (2014) 4792.
[47] R.T. Howie, P. Dalladay-Simpson and E. Gregoryanz, Raman spectroscopy of hot hydrogen above 200 GPa, *Nat. Mater.* **14** (2015) 495.
[48] P. Dalladay-Simpson, R.T. Howie and E. Gregoryanz, Evidence for a new phase of dense hydrogen above 325 gigapascals, *Nature* **529** (2016) 63.
[49] M.D. Knudson, M.P. Desjarlais, A. Becker, R.W. Lemke, K.R. Cochrane, M.E. Savage, D.E. Bliss, T.R. Mattsson and R. Redmer, Direct observation of an abrupt insulator-to-metal transition in dense liquid deuterium, *Science* **348** (2015) 1455.
[50] I.I. Naumov, R.E. Cohen and R.J. Hemley, Graphene physics and insulator–metal transition in compressed hydrogen, *Arxiv* (2013) 1305.4649v1.
[51] C.J. Pickard, M. Martinez-Canales and R.J. Needs, Density functional theory study of phase IV of solid hydrogen, *Arxiv* (2014) 1204.3304v2.
[52] A.E. Carlsson and N.W. Ashcroft, Approaches for reducing the insulator–metal transition pressure in hydrogen, *Phy. Rev. Lett.* **50** (1983) 1305.
[53] M.I. Eremets, I.A. Trojan, S.A. Medvedev, J.S. Tse and Y. Yao, Superconductivity in hydrogen dominant materials: silane, *Science* **319** (2008) 1506.
[54] Y. Xie, Q. Li, A.R. Oganov and H. Wang, Superconductivity of lithium-doped hydrogen under high pressure, *Acta Crystallogr.* **C70** (2014) 104.
[55] A.P. Drozdov, M.I. Eremets, I.A. Troyan, V. Ksenofontov and S.I. Shylin, Conventional superconductivity at 203 K at high pressures, *Arxiv* (2015) 1506.08190.
[56] T.F. Gallagher, *Rydberg Atoms*, Cambridge University Press, Cambridge, 1994.
[57] H. Shimizu, E.M. Brody, H.-K. Mao and P.M. Bell, Brillouin measurements of solid n-H2 and n-D2 to 200 kbar at room temperature, *Phys. Rev. Lett.* **47** (1981) 128.
[58] J. Wang and L. Holmlid, Formation of long-lived Rydberg states of H_2 at K impregnated surfaces, *Chem. Phys.* **261** (2000) 481.
[59] S. Muto, T. Tanabe and T. Maruyama, Cross sectional TEM observation of gas-ion-irradiation induced surface blisters and their precursors in SiC, *Mater. Trans.* **41** (2003) 2599.
[60] H. Cohen, P. Rez, T. Aoki, P.A. Crozier, N. Dellby, Z. Dellby, D. Gur, T.C. Lovejoy, K. March, M.C. Sarahan, S.G. Wolf and O.L. Krivanek, Hydrogen analysis by ultra-high energy resolution EELS, *Microsc. Microanal.* **21** (2015) 661.
[61] D.A. Tenne, A.K. Farrar, C.M. Brooks, T. Heeg, J. Schubert, H.W. Jang, C.W. Bark, C.M. Folkman, C.B. Eom and D.G. Schlom, Ferroelectricity in nonstoichiometric $SrTiO_3$ films studied by ultraviolet Raman spectroscopy, *Appl. Phys. Lett.* **97** (2010) 142901.